SCIENCE CHINA
Physics, Mechanics & Astronomy

•Article•

December 2018 Vol. 61 No. 12: 128711
https://doi.org/10.1007/s11433-018-9264-x

Entropic pressure between fluctuating membranes in multilayer systems

Long Li[1,2], Xiaohuan Wang[1], Yingfeng Shao[1,2], Wei Li[3], and Fan Song[1,2*]

[1] *State Key Laboratory of Nonlinear Mechanics (LNM) and Beijing Key Laboratory of Engineered Construction and Mechanobiology, Institute of Mechanics, Chinese Academy of Sciences, Beijing 100190, China;*
[2] *School of Engineering Science, University of Chinese Academy of Sciences, Beijing 100049, China;*
[3] *School of Mechanical and Electrical Engineering, North China Institute of Aerospace Engineering, Langfang 065000, China*

Received May 2, 2018; accepted June 13, 2018; published online August 10, 2018

Gaining insights into the fluctuation-induced entropic pressure between membranes that mediates cell adhesion and signal transduction is of great significance for understanding numerous physiological processes driven by intercellular communication. Although much effort has been directed toward investigating this entropic pressure, there still exists tremendous controversy regarding its quantitative nature, which is of primary interest in biophysics, since Freund challenged the Helfrich's well-accepted results on the distance dependence. In this paper, we have investigated the entropic pressure between fluctuating membranes in multilayer systems under pressure and tension through theoretical analysis and Monte Carlo simulations. We find that the scaling relations associated with entropic pressure depend strongly on the magnitude of the external pressures in both bending rigidity- and surface tension-dominated regimes. In particular, both theoretical and computational results consistently demonstrate that, in agreement with Helfrich, the entropic pressure p decays with inter-membrane separations c as $p\sim c^{-3}$ for the tensionless multilayer systems confined by small external pressures. However, our results suggest that the entropic pressure law follows to be $p\sim c^{-1}$ and $p\sim c^{-3}$, respectively, in the limit of large and small thermal wavelengths for bending fluctuations of the membranes in a tension-independent manner for the case of large external pressures.

entropic pressure, fluctuating membranes, statistical mechanics theory, Monte Carlo simulation, cell adhesion

PACS number(s): 87.16.A-, 87.16.D-, 87.16.dj, 87.16.Xa, 87.17.Rt

Citation: L. Li, X. Wang, Y. Shao, W. Li, and F. Song, Entropic pressure between fluctuating membranes in multilayer systems, Sci. China-Phys. Mech. Astron. **61**, 128711 (2018), https://doi.org/10.1007/s11433-018-9264-x

1 Introduction

Membranes play tremendously important roles in cells as selective barriers for maintaining concentrations and as functional platforms for crucial biological processes. They undergo thermal shape fluctuations in physiological conditions, resulting from the Brownian motion of the water molecules (see Figure 1). A single membrane fluctuates freely, and the mean value of membrane free energy remains constant. As two or more membranes approach each other, interactions between neighboring membranes sterically suppress the amplitude of their out-of-plane fluctuations. This confinement decreases the entropy of the membrane systems, and the ensuing increase in free energy gives rise to a distance-dependent repulsive pressure of entropic character that tends to push the membranes apart. As has been shown in many studies, this entropic pressure governs numerous cellular processes, e.g., cell adhesion, immune responses, as well as cell fusion [1-11].

*Corresponding author (email: songf@lnm.imech.ac.cn)

Stacks of lipid bilayers are optimal model systems for providing ideal environments to study the quantitative nature of the entropic pressure, which is of primary interest in biophysics, since the range of interbilayer distances can be systematically varied by applying osmotic pressure. Deducing from the dimensional considerations, Helfrich [12] proposed that the entropic pressure has a c^{-3} dependence for tensionless stacks in his pioneering work, where c is the mean separation between neighboring membranes in multilayer systems. Although some assumptions and simplifications were introduced in Helfrich's studies, his results were still supported by succeeding theories [13], simulations [14], as well as experiments [15]. However, based on the theories of elasticity and statistical mechanics, Freund found instead the entropic pressure to vary as c^{-1}, rather than the Helfrich's well-accepted result c^{-3} [16]. This result immediately triggered a series of disputes [17-20]. Subsequently, there have been two published simulation studies to address this discrepancy. Auth and Gompper [21] and Hanlumyuang et al. [22] showed that the distance dependence of the entropic pressure depends on the inter-membrane separation for the case of zero surface tension. They proposed that the results derived by Freund and Helfrich hold valid for small (c<0.4a $(k_{\mathrm{B}}T/\kappa)^{1/2}$) and intermediate ($0.4a(k_{\mathrm{B}}T/\kappa)^{1/2}$<$c$<$0.4L(k_{\mathrm{B}}T/\kappa)^{1/2}$) separations, respectively. However, their computational results are not in conformity with each other for large separations (c>$0.4L(k_{\mathrm{B}}T/\kappa)^{1/2}$) even though both the studies have adopted the same method (Monte Carlo simulation) for the same system (a single representative membrane of size $L \times L$ fluctuating between rigid planes). More specifically, Auth and Gompper [21] obtained a c^{-1} pressure law, but Hanlumyuang et al. [22] showed a $c^{-\eta}$ dependence with undetermined power η for large separations. Here, a denotes the discretization length, κ is the bending rigidity of the flexible membrane, k_{B} and T are the Boltzmann constant and the absolute temperature, respectively. However, using dissipative particle dynamics simulations, Vaiwala and Thaokar [23] recently theorized a pressure law, which follows Freund's prediction that the entropic pressure scales as c^{-1}. It remains an intriguing open problem to determine the quantitative nature of the entropic pressure. More importantly, the effect of the surface tension, which biological and biomimetic membranes often experience, on the entropic pressure also needs to be further investigated.

In this paper, we have studied the entropic pressure between membranes in a periodic stack under external pressure and surface tension by theoretical analysis and Monte Carlo simulations. We have considered two cases where the thermal shape fluctuations of the flexible membranes are dominated by bending rigidity and surface tension, respectively. It is found that the scaling relations between entropic pressure and characteristic parameters used to describe the membrane fluctuations depend strongly on the magnitude of the external pressures in both rigidity- and tension-dominated regimes. In particular, the distance dependence of entropic pressure p for the tension-free multilayer system is c^{-3} for small pressures, verified consistently by both theory and simulations. Further increase in external pressure changes the p–c dependence. It indicates that the distance dependence of the entropic pressure does not depend on the surface tension and follows to be p~c^{-1} and p~c^{-3}, respectively, in the limit of large and small thermal wavelengths for bending fluctuations of the membranes in the large-pressure regime.

2 Theoretical model

Consider a single membrane confined by neighboring membranes within a multilayer system subjected to external pressure and surface tension. The thermally driven out-of-plane fluctuations of the membrane can be characterized by correlation lengths $\xi_{\parallel}$ and $\xi_{\perp}$, as shown in Figure 1. The parallel correlation length $\xi_{\parallel}$ is interpreted as the average size of the largest membrane humps, and perpendicular correlation length (or roughness) $\xi_{\perp}$ gives their amplitude [21,24]. Each such hump has a volume $V \simeq \xi_{\perp}\xi_{\parallel}^{2}$. The two length scales can be derived from the height-height correlation function $C(r,r') = \langle h(r)h(r')\rangle$ with parallel correlation length $\xi_{\parallel}$ defined by $C(r,r') \sim \exp\left(-|R|/\xi_{\parallel}\right)$ and roughness $\xi_{\perp}^{2} = C(R=0)$. Here, $h(\mathbf{r})$ measures the membrane displacement related to the reference plane at position $\mathbf{r} = (x, y)$, $R = r - r'$.

In order to determine $\xi_{\parallel}$ and $\xi_{\perp}$, we adopt the interaction potential $V(h(r))$ to describe the confinement which the membranes experience due to the presence of external pressure. As confirmed previously [21,25], the confining potential can be well approximated by a parabolic potential $V(h(r))$=$vh^2/2$ with potential strength v. The effective Hamiltonian of the confined membrane is then written as:

$$H = \int \mathrm{d}r \left\{ \frac{1}{2}vh^2 + \frac{1}{2}\tau(\nabla h)^2 + \frac{1}{2}\kappa(\nabla^2 h)^2 \right\}, \quad (1)$$

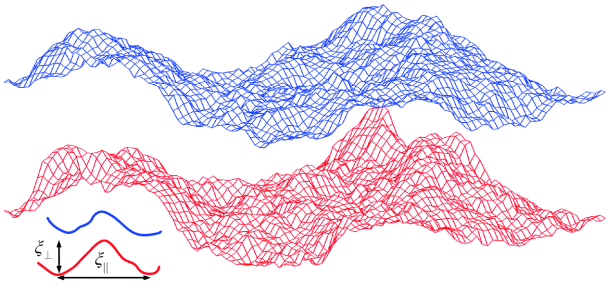

Figure 1 (Color online) Two interacting membranes in a stack undergo thermal shape fluctuations characterized by the parallel correlation length $\xi_{\parallel}$ and perpendicular correlation length $\xi_{\perp}$.

where τ denotes the lateral tension.

We proceed by expanding $h(\mathbf{r})$ in Fourier modes on a square piece of membrane of area $A = L \times L$ with periodic boundary conditions

$$h(\mathbf{r}) = \sum_{\mathbf{q}} h_{\mathbf{q}} \exp(\mathrm{i}\mathbf{q}\cdot\mathbf{r}), \tag{2}$$

where i is the imaginary unit, $\mathbf{q}=(2\pi/L)(m, n)$ with $m, n \in \mathbb{Z}$. Since $h(r)$ is a real function, the amplitude of the wave satisfies $h_{-\mathbf{q}} = h_{\mathbf{q}}^*$, in which the star denotes complex conjugation. We use the Fourier representation of eq. (2) to write the $h(\mathbf{r})$ terms as:

$$\begin{aligned} h^2 &= \sum_{\mathbf{q},\mathbf{q}'} h_{\mathbf{q}} h_{\mathbf{q}'} \exp[\mathrm{i}(\mathbf{q}+\mathbf{q}')\cdot\mathbf{r}], \\ (\nabla h)^2 &= \sum_{\mathbf{q},\mathbf{q}'} h_{\mathbf{q}} h_{\mathbf{q}'} (-\mathbf{q}\cdot\mathbf{q}') \exp[\mathrm{i}(\mathbf{q}+\mathbf{q}')\cdot\mathbf{r}], \\ (\nabla^2 h)^2 &= \sum_{\mathbf{q},\mathbf{q}'} h_{\mathbf{q}} h_{\mathbf{q}'} (q^2 q'^2) \exp[\mathrm{i}(\mathbf{q}+\mathbf{q}')\cdot\mathbf{r}]. \end{aligned} \tag{3}$$

With the kronecker-δ function $\delta_{q,0} = A^{-1}\int \exp(-\mathrm{i}q\cdot r)\mathrm{d}r$ expressed in terms of the Fourier representation, the effective Hamiltonian is given by

$$\begin{aligned} H &= A\sum_{q}\left(\frac{v+\tau q^2+\kappa q^4}{2}\right) h_q h_q^* \\ &= A\sum_{q}\left(\frac{v+\tau q^2+\kappa q^4}{2}\right) \left| h_q \right|^2 \end{aligned} \tag{4}$$

upon inserting eq. (3) into eq. (1). Invoking the equipartition theorem, we immediately find for the height fluctuation spectrum

$$\left\langle \left| h_{\mathbf{q}} \right|^2 \right\rangle = \frac{k_{\mathrm{B}}T}{A\left(v+\tau q^2+\kappa q^4\right)}, \tag{5}$$

where the angular brackets denote the ensemble average. Applying the Fourier transform to $h_{\mathbf{q}}$, one obtains the correlation function

$$\begin{aligned} C(\mathbf{r},\mathbf{r}') &= \langle h(\mathbf{r})h(\mathbf{r}')\rangle \\ &= \frac{1}{A}\sum_{\mathbf{q},\mathbf{q}'}\left\langle h_{\mathbf{q}} h_{\mathbf{q}'}\right\rangle \exp[\mathrm{i}(\mathbf{q}\cdot\mathbf{r}+\mathbf{q}'\cdot\mathbf{r}')] \\ &= \frac{1}{A}\sum_{\mathbf{q}} \mathrm{e}^{\mathrm{i}\mathbf{q}\cdot R}\frac{k_{\mathrm{B}}T}{v+\tau q^2+\kappa q^4} \\ &= \frac{1}{4\pi^2}\int \mathrm{d}\mathbf{q}\mathrm{e}^{\mathrm{i}\mathbf{q}\cdot R}\frac{k_{\mathrm{B}}T}{v+\tau q^2+\kappa q^4} \\ &= \frac{1}{4\pi^2}\int_0^{\infty}\int_0^{2\pi} q\mathrm{e}^{\mathrm{i}qR\cos\theta}\mathrm{d}q\mathrm{d}\theta\frac{k_{\mathrm{B}}T}{v+\tau q^2+\kappa q^4} \\ &= \frac{k_{\mathrm{B}}T}{2\pi}\int_0^{\infty}\mathrm{d}q\frac{qJ_0(qR)}{v+\tau q^2+\kappa q^4}, \end{aligned} \tag{6}$$

where use has been made of the kronecker-δ function and Bessel function $J_0(qR) = \frac{1}{2\pi}\int_0^{2\pi}\mathrm{e}^{\mathrm{i}qR\cos\theta}\mathrm{d}q$.

By definition, one obtains the exact relation

$$\begin{aligned} \xi_{\perp}^2 &= \langle h(\mathbf{r})h(\mathbf{r})\rangle = \int\frac{\mathrm{d}\mathbf{q}}{(2\pi)^2}\frac{k_{\mathrm{B}}T}{v+\tau q^2+\kappa q^4} \\ &= \frac{k_{\mathrm{B}}T}{2\pi\tau}\frac{1}{\sqrt{\left|1-4v\kappa/\tau^2\right|}} \\ &\quad\cdot\begin{cases} \arctan\sqrt{4v\kappa/\tau^2-1}, & \text{for } \tau^2<4v\kappa, \\ \dfrac{1}{2}\ln\dfrac{1+\sqrt{1-4v\kappa/\tau^2}}{1-\sqrt{1-4v\kappa/\tau^2}}, & \text{for } \tau^2>4v\kappa. \end{cases} \end{aligned} \tag{7}$$

It then follows that the roughness scales as:

$$\xi_{\perp}^2 \to \begin{cases} \dfrac{k_{\mathrm{B}}T}{8\sqrt{v\kappa}}, & \text{for } \tau^2 \ll 4v\kappa, \\ \dfrac{k_{\mathrm{B}}T}{2\pi\tau}\ln\left(\dfrac{\tau}{\sqrt{v\kappa}}\right), & \text{for } \tau^2 \gg 4v\kappa, \end{cases} \tag{8}$$

for rigidity-dominated and tension-dominated regimes. Similar calculations can be carried out for the parallel correlation length $\xi_{\parallel}$, yielding

$$\xi_{\parallel} \to \begin{cases} (4\kappa/v)^{1/4}, & \text{for } \tau^2 \ll 4v\kappa, \\ \sqrt{\tau/v}, & \text{for } \tau^2 \gg 4v\kappa. \end{cases} \tag{9}$$

When this relation is combined with eq. (8), one obtains the length scales $\xi_{\perp}$ and $\xi_{\parallel}$ satisfying

$$\xi_{\perp}^2 = \begin{cases} \dfrac{k_{\mathrm{B}}T}{16\kappa}\xi_{\parallel}^2, & \text{for } \tau^2 \ll 4v\kappa, \\ \dfrac{k_{\mathrm{B}}T}{2\pi\tau}\ln\left(\xi_{\parallel}\sqrt{\dfrac{\tau}{\kappa}}\right), & \text{for } \tau^2 \gg 4v\kappa, \end{cases} \tag{10}$$

within the rigidity-dominated and tension-dominated regimes.

Using the ideal gas law $pV = k_{\mathrm{B}}T$ for each hump of longitudinal and transverse dimensions $\xi_{\parallel}$ and $\xi_{\perp}$ together with eq. (10), we can obtain the scaling relations

$$\begin{cases} \langle h\rangle = c \sim \xi_{\perp} \sim \xi_{\parallel} \sim 1/p^{1/3}, & \text{for } \tau^2 \ll 4v\kappa, \\ \hat{c} + \ln(\hat{c}^{1/4}) \sim \tau\xi_{\perp}^2 \sim \ln\left(\xi_{\parallel}^2\tau/\kappa\right) \sim & \\ -\ln\left(pL^2/\sqrt{k_{\mathrm{B}}T\tau}\right), & \text{for } \tau^2 \gg 4v\kappa, \end{cases} \tag{11}$$

where we have used $c/\xi_{\perp} = \sqrt{5}$ [26] and $4\pi\tau\xi_{\perp}^2/k_{\mathrm{B}}T \approx \hat{c} + \ln(\hat{c})/4$ with $\hat{c} = c/\sqrt{k_{\mathrm{B}}T/\pi\tau}$ [27] for the two limiting situations of vanishing surface tension and bending rigidity. Eq. (11) clearly indicates that the entropic pressure varies as c^{-3} for tensionless stacks of membranes, which is consistent with Helfrich's result. Meanwhile, as we can see, the surface tension has a significant impact on the pressure law, since it reduces the thermal shape fluctuations of the membrane and thus suppresses the fluctuation-induced repulsion.

3 Monte Carlo simulations

3.1 Model and method

Four types of entropic forces between biomembranes have

been identified: protrusion, headgroup overlap, peristaltic and undulation forces [28]. The first two arise from molecular-scale fluctuations. They can be influenced by the hydration forces and the molecular structure of the lipid-water interface should be taken into account on this length scale [29,30]. By contrast, the last two arise from collective motions of biomembranes on length scales which are large compared to the membrane thickness. They can be described in terms of their continuum elastic modulus, respectively. Therefore, we should carefully choose the appropriate simulation models at different scales to investigate the four types of entropic forces. Here, we focus on the last force and view the membrane as a thin elastic sheet (Figure 2(a)), neglecting the detailed molecular structures. In this section, Monte Carlo simulations are employed to study the undulation-induced entropic pressure in a multilayer system consisting of a stack of N interacting membranes bound by an external pressure p. The n-th membrane surface governed by bending rigidity κ_n and lateral tension τ_n can be parameterized by the height profile $h_n(\mathbf{r})$. Since the neighboring membranes cannot overlap each other, so that $h_1 < h_2 < \cdots < h_N$. In the Monte Carlo simulations, the interacting membranes are represented by two dimensional square lattices of spacing a (see Figure 2(a)). The effective Hamiltonian then takes the form

$$H = \sum_{n=1}^{N}\sum_{r}\left[\frac{\kappa_n}{2a^2}\left(\nabla_{\mathrm{d}}^2 h_n(r)\right)^2 + \frac{\tau_n}{2}\left(\nabla_{\mathrm{d}} h_n(r)\right)^2\right] + \sum_{r} a^2\left[p(h_N(r) - h_1(r))\right], \tag{12}$$

where $\nabla_d^2 h_n(r)$ is the discrete Laplacian of the local membrane separation $h_n(\mathbf{r})$, $\left(\nabla_d h_n(r)\right)^2$ describes the increase of membrane area per unit projected area. In our simulations, local moves with a random step size δc are attempted at all lattices to generate new membrane configurations using standard Metropolis algorithm shown in eq. (13)

$$\Re(\text{old} \to \text{new}) = \begin{cases} \exp(-\Delta H / k_{\mathrm{B}}T), & \text{if } \Delta H > 0, \\ 1, & \text{otherwise}, \end{cases} \tag{13}$$

where $\Re(\text{old} \to \text{new})$ is the Metropolis acceptance ratio, and the energy difference ΔH between the old and new membrane configurations is given by

$$\Delta H = \frac{\kappa}{a^2}\delta c\left[10\left(2h_\chi + \delta c\right) - 8\sum h_{\langle\chi\rangle} + 2\sum h_{[\chi]} + \sum h_{\{\chi\}}\right] + \tau\left\{\delta c\left(4h(r) - \sum h_{\langle\chi\rangle} + 2\delta c\right)\right\} + \theta a^2 p\delta c \tag{14}$$

with

$$\theta = \begin{cases} -1, & n = 1, \\ 1, & n = N, \\ 0, & \text{otherwise}. \end{cases} \tag{15}$$

Here, $\langle\chi\rangle$, $[\chi]$, and $\{\chi\}$ denote the first, second, and third nearest neighbors of a randomly selected lattice χ, respectively (see Figure 2(b)). We simulate the membranes each composed of 60×60 patches in a cubic box under periodic boundary conditions. In each Monte Carlo step, an attempted local move for all membrane patches is accomplished. In our study, we perform 107 Monte Carlo steps to leave the system in equilibrium, and average the physical quantities of interest during the subsequent 5×107 Monte Carlo steps.

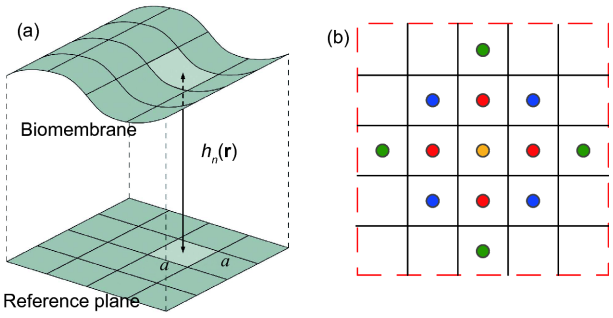

Figure 2 (Color online) (a) Discretized model of a fluctuating membrane. The membrane is divided up into quadratic lattices with projected area $a \times a$. The configurations of the n-th fluctuating membrane are described by the transverse deflection $h_n(\mathbf{r})$ related to the reference plane. (b) Neighbors of a selected lattice marked by a golden dot. The nearest neighbors are marked by the red dots, the second nearest neighbors by the blue dots, and the third nearest neighbors by the green dots.

3.2 Simulation results and discussion

3.2.1 *Tensionless stacks of interacting membranes*

We consider first the case in which a stack of fluctuating membranes with identical bending rigidity $\kappa_n \equiv \kappa$ is confined by external pressure p in the absence of surface tension. For a stack of two membranes as shown in Figure 3(a), we estimate roughness $\xi_\perp$ from $\langle(h_2 - h_1 - \langle h\rangle)^2\rangle^{1/2}$, parallel correlation length $\xi_\parallel$ from $a\exp[(2\pi(\kappa / k_{\mathrm{B}}T)\ \langle(\nabla h)^2\rangle]$ [24]. By performing Monte Carlo simulations, we find two power-law regimes. From Figure 4(a), a good agreement between simulation and theory for the scaling relations between mean separation $\langle h\rangle = c$, roughness $\xi_\perp$, parallel correlation length $\xi_\parallel$ and entropic pressure p is clearly observed for small pressures. However, these scaling laws derived theoretically in eq. (11) for the bending rigidity-dominated regime gradually no longer hold true as the external pressure rises, and are replaced by

$$\langle h\rangle = c \approx \xi_\perp,\ \xi_\parallel \approx a,\ c = k_{\mathrm{B}}T / a^2 p \tag{16}$$

for large pressures, where the distance dependence of the entropic pressure (the third term in eq. (16)) is obtained using the ideal gas law $pV = k_{\mathrm{B}}T$. We further perform simulations for a stack of three tensionless membranes (see Figure 3(b)). Figure 4(b) shows the ratio of mean separations for stacks of three and two membranes, which gradually reaches unity with increasing external pressure. This implies that the entropic pressure law obtained in eq. (16) is completely independent of the number of membranes in a stack for large

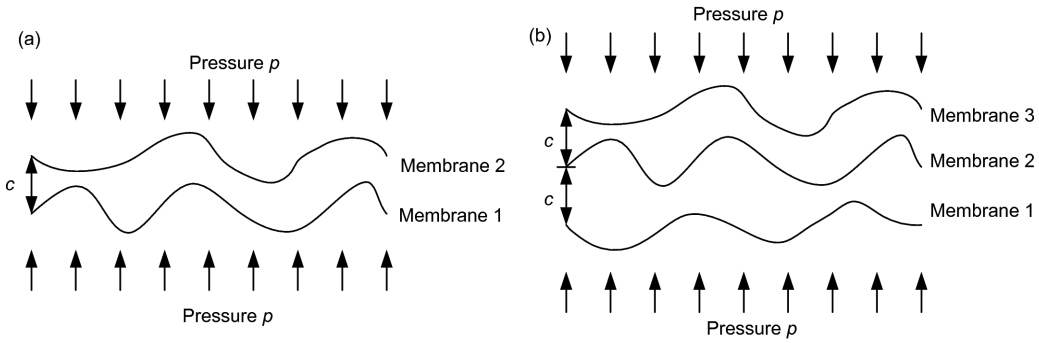

Figure 3 A stack of (a) two and (b) three tensionless membranes under external pressure.

pressures. The crossover external pressure can be obtained by equating the pressure law in eq. (16) and Helfrich's pressure law of $p = \omega\,(k_BT)^2/(\kappa c^{-3})$ with coefficient $\omega = 0.22$ determined from the Monte Carlo data in Figure 4(a), which is given by

$$p_{be} \approx 2.1(k_BT\kappa)^{1/2}a^{-3} \tag{17}$$

for the case where the membrane fluctuations are dominated by the bending rigidity.

At first sight, one might conclude from eq. (16) that the entropic pressure has a c^{-1} dependence. However, the role of the discretization length a should be seriously taken into account. As shown in Figure 4(c), the scaling relations between three characteristic parameters and entropic pressure are a-independent for small pressures ($p < p_{be}$), but show an a-dependent manner for large pressures ($p > p_{be}$). It can be clearly seen that the mean separation between membranes varies with the discretization length a even for the same external pressure p when $p > p_{be}$. By comparing directly the entropic pressure law derived in eq. (16) for the case of large pressures ($p > p_{be}$) with that of Freund [16], we find that the discretization length a corresponds to the thermal wavelength λ in Freund's model. We now focus on two extreme cases of the entropic pressure in eq. (16). First, let us consider the case where the membranes only generate a single wave under the entropic pressure. At this time, the wave-

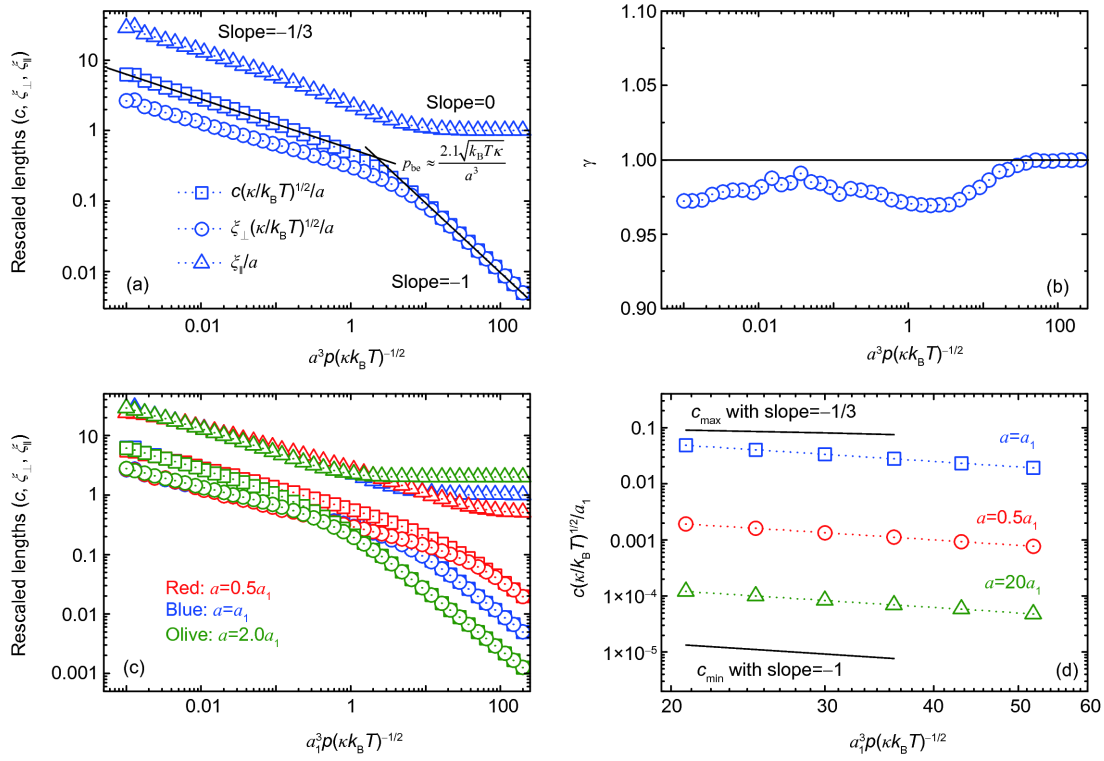

Figure 4 (Color online) Monte Carlo simulation results for tensionless membranes. (a) Three rescaled characteristic parameters as a function of the rescaled pressure in a log-log format for a stack of two membranes; (b) ratio γ of mean separations for stacks of three and two identical membranes as a function of the rescaled pressure; (c) three characteristic parameters as a function of the rescaled pressure for a stack of two membranes with different discretization lengths indicated by different colors: red for $a = 0.5a_1$, blue for $a = a_1$, and olive for $a = 2.0a_1$. The meaning of all symbols is the same as in (a); (d) the lower and upper bounds of the mean separation for large pressures.

length of the wave will reach its maximum value $\lambda = \lambda_{\max} = L$, and accordingly the parallel correlation length $\xi_{\parallel} = a = L$. This leads to

$$c_{\min} = \frac{k_{\mathrm{B}}T}{L^2 p}, \tag{18}$$

showing that the entropic pressure varies as c^{-1} for large pressures. Obviously, eq. (18) forms the lower bound of the p–c dependence derived in eq. (16) (see Figure 4(d)), which manifests that the mutual steric hindrance of undulating membranes in multilayer systems reaches the minimum. Next, let us consider another extreme case where the fluctuating membranes generate waves with smallest wavelengths $\lambda = \lambda_{\min}$ response to the entropic pressure. To proceed, we let the dimensions of a membrane approach to $\lambda_{\min}$. In this case, the membrane is similar to a single molecule that undergoes random vibrations in the transverse direction. At this time, we obtain the bending energy of one small square tensionless membrane with lateral size $\lambda_{\min}$ to be $H_{\mathrm{B}} = 8\pi^4\kappa \left|h_q\right|^2 / \lambda_{\min}^2$ with $\mathbf{q} = (2\pi/\lambda_{\min}, 2\pi/\lambda_{\min})$. Equating the average energy $\langle H_{\mathrm{B}}\rangle$ to $k_{\mathrm{B}}T$, together with the thermal expectation $\left\langle \left|h_q\right|^2 \right\rangle = c^2/12$ [31], gives $\lambda_{\min}^2 = 2\pi^4\kappa c^2 / 3k_{\mathrm{B}}T$. Substituting this expression for $\lambda_{\min}$ into the third term in eq. (16) yields the entropic pressure law for the case of $\xi_{\parallel} = a = \lambda_{\min}$,

$$c_{\max}^3 = \frac{3(k_{\mathrm{B}}T)^2}{2\pi^4\kappa p}, \tag{19}$$

showing that the entropic pressure varies as c^{-3} for large pressures. Obviously, eq. (19) forms the upper bound of the p–c dependence derived in eq. (16) (see Figure 4(d)), which indicates that the mutual steric hindrance of undulating membranes in multilayer systems reaches the maximum.

Previous studies mainly focus on the p–c dependence in the small-pressure regime and neglect the role of the thermal wavelengths for bending fluctuations of the membranes in the distance dependence of the undulation-induced pressure. The simulation results above indicate that the distance dependence of the entropic pressure depends strongly on the magnitude of the external pressures. The entropic pressure indeed follows a c^{-3} behavior for small pressures ($p < p_{\mathrm{be}}$). However, the p–c dependence is closely related to the discretization length a, which corresponds to the wavelength λ in the work by Freund, for large pressures ($p > p_{\mathrm{be}}$). It illustrates that the entropic pressure depends on the inverse distance and cubed inverse distance for large and small discretization lengths, respectively, in this regime.

3.2.2 *Stacks of interacting membranes under surface tension*

Attention is now turned to the case where the membranes in a stack confined by external pressures experience surface tensions τ. To proceed, we carry out simulations for a pair of identical membranes (Figure 5) with ten-fold serial tensions $\hat{\tau}$ ranging from 0.002 to 200, where $\hat{\tau} = a^2\tau/\kappa$ is the rescaled membrane surface tension. As expected, from the results presented in Figure 6(a) and (b), we can see that the scaling relations $\langle h\rangle \sim c \sim \xi_{\perp} \sim 1/p^{1/3}$ derived theoretically in eq. (11) still hold true for small surface tensions in the small-pressure regime, where the thermal fluctuations of the membranes are governed by the bending rigidity. Owing to the inhibitory effect of surface tension on the thermal shape fluctuations of membranes in a stack and on the fluctuation-induced steric repulsion, the scaling relations change with increasing surface tension. As shown in Figure 6(c), the theoretical result $pa^2/\sqrt{k_{\mathrm{B}}T\tau} = \hat{p} \approx \psi\exp(-\hat{c})\hat{c}^{-1/4}$ derived in eq. (11) for the tension-dominated regime is validated by finding good agreement with our Monte Carlo simulations, and the coefficient ψ is estimated as $\psi \approx 2.6$. In addition, it is revealed that the linear relation $\langle h\rangle/\xi_{\perp} = 5^{1/2}$ [26] for tensionless multilayer systems shows a pressure-related manner due to the presence of surface tension τ, and follows to be $\langle h\rangle/\xi_{\perp} \sim -\varphi a^3 p(\kappa k_{\mathrm{B}}T)^{-1/2}$ with $\varphi \approx 0.65$ for large τ in the small-pressure regime (see Figure 6(d)). Nevertheless, as clearly illustrated in Figure 6(a)-(c), these above-mentioned scaling laws gradually fail to describe the behavior of interacting membranes with further increase in external pressure. Surprisingly, we find that the scaling relation between mean separation and membrane roughness, and the distance dependence of entropic pressure follow to be $\langle h\rangle/\xi_{\perp} \approx 1$ and $c = k_{\mathrm{B}}T/a^2p$, respectively, even in the presence of large tensions, which are the same as those given by eq. (16). This implies that the lateral surface tension has little effect on the scaling relations between three characteristic parameters and entropic pressure in the large-pressure regime. The crossover external pressure can be obtained by equating the pressure laws $pa^2/\sqrt{k_{\mathrm{B}}T\tau} \approx 2.6\exp(-\hat{c})\hat{c}^{-1/4}$ and $c = k_{\mathrm{B}}T/a^2p$, which is given by

$$p_{\mathrm{te}} \approx 1.3(k_{\mathrm{B}}T\pi\tau)^{1/2}a^{-2} \tag{20}$$

for the case where the membrane fluctuations are dominated by the surface tension.

As shown above, the theoretical predictions of scaling

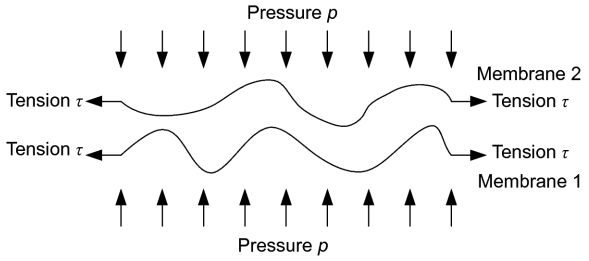

Figure 5 A stack of two interacting membranes under external pressure and surface tension.

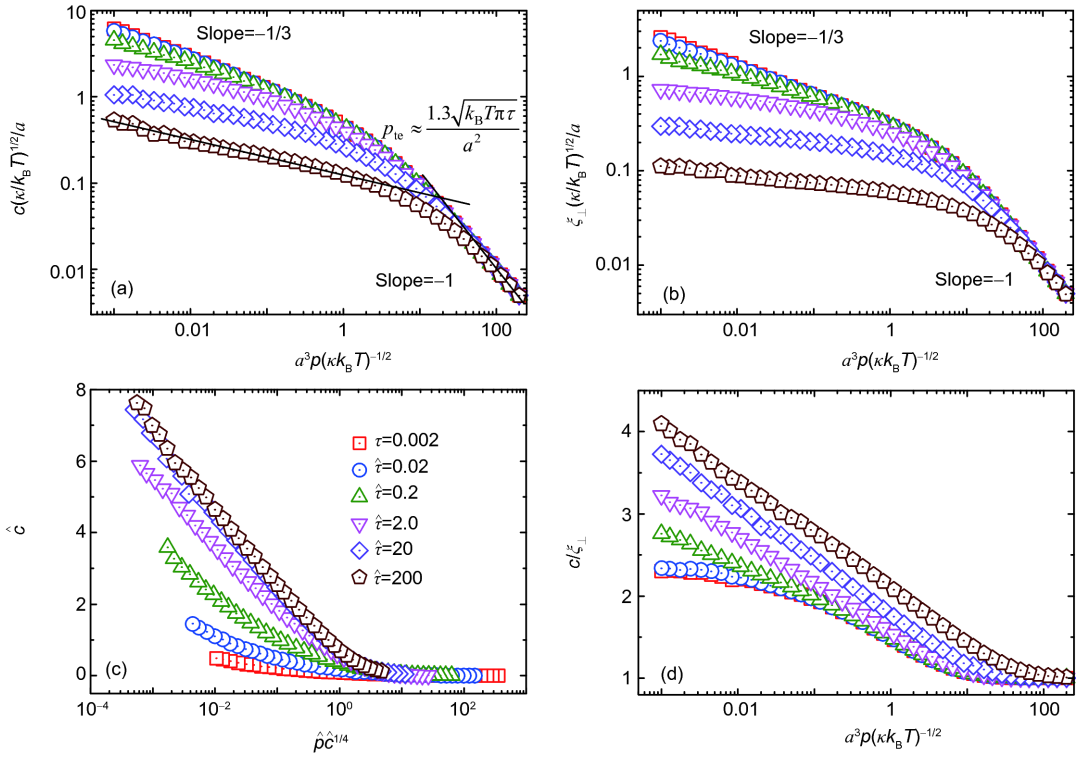

Figure 6 (Color online) Monte Carlo simulation results for a stack of two membranes with different surface tensions showing (a) mean separation c, (b) roughness $\xi_\perp$, (c) rescaled mean separation $\hat{c}$, as well as (d) mean separation/roughness ratio as a function of the rescaled pressure.

relations are in good agreement with those obtained by Monte Carlo simulations for both rigidity- and tension-dominated regimes when the external pressures are small, while discrepancy occurs in the large-pressure regime. This discrepancy is essentially attributed to the form of the confining potential adopted in the theoretical analysis. To quantitatively analyze the fluctuation-induced interaction, we employ a parabolic potential as given by $V(h(\mathbf{r})) = vh^2/2$ to mimic the confinement of external pressures. Accordingly, the distribution of density profile and height field of the membrane is Gaussian, which agrees well with the simulation results for a stack of membranes under small pressures [21,25], thus justifying the harmonic approximation for the confining potential. Nevertheless, the membrane density profile has been shown to be pressure-dependent, and does not follow a Gaussian distribution any more for large pressures [21]. Therefore, the harmonic approximation for the confining potential is no longer appropriate, which leads to a consequence that the theoretical predictions as given in eq. (11) fail to describe the fluctuation-induced interactions of the membranes in a stack.

4 Conclusions

We have systematically investigated the fluctuation-induced entropic pressure between fluid membranes in multilayer systems by using statistical mechanics theory and Monte Carlo simulations. We find that the scaling relations between three characteristic parameters (mean separation c, roughness $\xi_\perp$, parallel correlation length $\xi_\parallel$) and entropic pressure are closely related to the magnitude of the external pressures. The crossover external pressures are determined to be $p_{be} \approx 2.1(k_B T\kappa)^{1/2}a^{-3}$ and $p_{te} \approx 1.3(k_B T\pi\tau)^{1/2}a^{-2}$ for the cases where the membrane fluctuations are dominated by the bending rigidity and surface tension, respectively. In the small-pressure regime, the theoretical predictions are validated by direct comparison with Monte Carlo simulation results for the cases where the membrane shape fluctuations are dominated by either bending rigidity or surface tension. In the large-pressure regime, we obtain new scaling laws to describe the fluctuation-induced interactions within the multilayer system. Particularly, the p–c dependence for tensionless membrane systems is found to be consistent with Helfrich's results showing that p scales as $p\sim c^{-3}$ for small pressures. However, this well-accepted distance dependence of entropic pressure changes with further increase in external pressure. It suggests that the mean separation has the lower and upper bounds which scale as $p\sim c^{-1}$ and $p\sim c^{-3}$, respectively, in a tension-independent manner for large pressures. We propose that the mean separation may exhibit oscillatory behaviors in the large-pressure regime. Our results provide novel insights

into the fluctuation-induced entropic pressure and help to reconcile the discrepancy between Helfrich's and Freund's results.

This work was supported by the National Natural Science Foundation of China (Grant Nos. 11472285, and 11572326), the Strategic Priority Research Program of the Chinese Academy of Sciences (Grant No. XDB22040102), and the National Key Research and Development Program of China (Grant No. 2016YFA0501601).

1 G. K. Xu, J. Qian, and J. Hu, Soft Matter **12**, 4572 (2016).
2 L. Li, J. Hu, X. Shi, Y. Shao, and F. Song, Soft Matter **13**, 4294 (2017).
3 L. Li, G. K. Xu, and F. Song, Phys. Rev. E **95**, 012403 (2017).
4 L. Li, J. Hu, G. Xu, and F. Song, Phys. Rev. E **97**, 012405 (2018).
5 H. Gao, J. Qian, and B. Chen, J. R. Soc. Interface **8**, 1217 (2011).
6 W. L. Zhang, J. Qian, H. M. Yao, W. Q. Chen, and H. J. Gao, Sci. China-Phys. Mech. Astron. **55**, 980 (2012).
7 S. F. Fenz, T. Bihr, D. Schmidt, R. Merkel, U. Seifert, K. Sengupta, and A. S. Smith, Nat. Phys. **13**, 906 (2017).
8 J. Hu, R. Lipowsky, and T. R. Weikl, Proc. Natl. Acad. Sci. USA **110**, 15283 (2013).
9 P. Tarazona, E. Chacón, and F. Bresme, J. Chem. Phys. **139**, 094902 (2013).
10 J. C. Wei, and F. Song, Sci. China-Phys. Mech. Astron. **60**, 014621 (2017).
11 J. Wang, Y. G. Shen, F. Song, F. J. Ke, Y. L. Bai, and C. S. Lu, Sci. China-Phys. Mech. Astron. **59**, 634602 (2016).
12 W. Helfrich, Z. Naturfors. Sect. A **33**, 305 (1978).
13 B. Kastening, Phys. Rev. E **73**, 011101 (2006).
14 R. R. Netz, and R. Lipowsky, Europhys. Lett. **29**, 345 (1995).
15 S. Bulut, I. Åslund, D. Topgaard, H. Wennerström, and U. Olsson, Soft Matter **6**, 4520 (2010).
16 L. B. Freund, Proc. Natl. Acad. Sci. USA **110**, 2047 (2013).
17 P. Sharma, Proc. Natl. Acad. Sci. USA **110**, 1976 (2013).
18 H. Wennerström, U. Olsson, and J. N. Israelachvili, Proc. Natl. Acad. Sci. USA **110**, E2944 (2013).
19 L. B. Freund, Proc. Natl. Acad. Sci. USA **110**, E2945 (2013).
20 H. Wennerström, and U. Olsson, Adv. Colloid Interface Sci. **208**, 10 (2014).
21 T. Auth, and G. Gompper, Phys. Rev. E **88**, 010701(R) (2013), arXiv: 1307.0647.
22 Y. Hanlumyuang, L. Liu, and P. Sharma, J. Mech. Phys. Solids **63**, 179 (2014), arXiv: 1307.1807.
23 R. Vaiwala, and R. Thaokar, EPL **120**, 48001 (2017).
24 R. Lipowsky, and B. Zielinska, Phys. Rev. Lett. **62**, 1572 (1989).
25 F. Córdoba-Valdés, R. Castañeda-Priego, J. Timmer, and C. Fleck, Soft Matter **10**, 8475 (2014).
26 R. R. Netz, Phys. Rev. E **51**, 2286 (1995).
27 R. Lipowsky, and S. Grotehans, BioPhys. Chem. **49**, 27 (1994).
28 J. N. Israelachvili, and H. Wennerstroem, J. Phys. Chem. **96**, 520 (1992).
29 J. Yin, and Y. P. Zhao, J. Colloid Interface Sci. **329**, 410 (2009).
30 M. Kanduč, E. Schneck, and R. R. Netz, Langmuir **29**, 9126 (2013).
31 W. Helfrich, and R. M. Servuss, Il Nuovo Cimento D **3**, 137 (1984).